Acta Crystallographica Section F
Structural Biology and Crystallization Communications
ISSN 1744-3091

X-ray structure and characterization of carbamate kinase from the human parasite *Giardia lamblia*

Andrey Galkin,[a] Liudmila Kulakova,[a] Rui Wu,[b] Theodore E. Nash,[c] Debra Dunaway-Mariano[b] and Osnat Herzberg[a]*

[a]W. M. Keck Laboratory for Structural Biology, Center for Advanced Research in Biotechnology, University of Maryland Biotechnology Institute, Rockville, Maryland, USA, [b]Department of Chemistry and Chemical Biology, University of New Mexico, Albuquerque, New Mexico, USA, and [c]Laboratory of Parasitic Diseases, National Institute of Allergy and Infectious Diseases, National Institutes of Health, Bethesda, Maryland, USA

Correspondence e-mail: herzberg@umbi.umd.edu

Received 10 December 2009
Accepted 5 February 2010

PDB Reference: carbamate kinase, 3kzf.

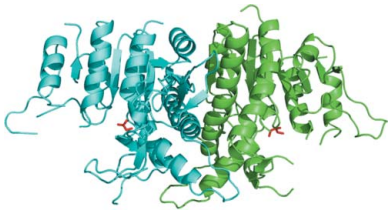

Carbamate kinase catalyzes the reversible conversion of carbamoyl phosphate and ADP to ATP and ammonium carbamate, which is hydrolyzed to ammonia and carbonate. The three-dimensional structure of carbamate kinase from the human parasite *Giardia lamblia* (*gl*CK) has been determined at 3 Å resolution. The crystals belonged to the monoclinic space group $P2_1$, with unit-cell parameters $a = 69.77$, $b = 85.41$, $c = 102.1$ Å, $\beta = 106.8^\circ$. The structure was refined to a final R factor of 0.227. The essentiality of *gl*CK together with its absence in humans makes the enzyme an attractive candidate for anti-*Giardia* drug development. Steady-state kinetic rate constants have been determined. The k_{cat} for ATP formation is 319 ± 9 s^{-1}. The K_m values for carbamoyl phosphate and ADP are 85 ± 6 and 70 ± 5 μM, respectively. The structure suggests that three invariant lysine residues (Lys131, Lys216 and Lys278) may be involved in the binding of substrates and phosphoryl transfer. The structure of *gl*CK reveals that a glycerol molecule binds in the likely carbamoyl phosphate-binding site.

1. Introduction

Carbamate kinase (CK; EC 2.7.2.2; ATP:carbamate phosphotransferase) from the arginine dihydrolase pathway catalyzes the reversible conversion of carbamoyl phosphate and ADP to ATP and ammonium carbamate, which is hydrolyzed to ammonia and carbonate. The three-step arginine dihydrolase pathway, involving arginine deiminase, ornithine transcarbamoylase and CK, is used by a number of microorganisms, including *Giardia lamblia*, to generate ATP (Biagini *et al.*, 2003; Knodler *et al.*, 1998). *G. lamblia* is the causative agent of the human intestinal disease giardiasis (for a review, see Adam, 2001), the most common cause of waterborne outbreaks of diarrhea in the United States. Infections are prevalent in impoverished countries, leading to much suffering and mortality. Because the arginine dihydrolase pathway is absent in humans and other high eukaryotes, the enzymes of this pathway are potential targets for drug development. Arginine deiminase and ornithine transcarbamoylase have been shown to be among the major proteins released into the medium after brief interaction of *G. lamblia* with human intestinal epithelial cells, underscoring the importance of the arginine catabolism pathway in host colonization by the parasite (Palm *et al.*, 2003). The *G. lamblia* CK (*gl*CK) was found to be the most active of the arginine dihydrolase enzymes, with a maximal activity in cell-free extracts that was fivefold to tenfold greater than those of arginine deiminase and ornithine transcarbamoylase (Schofield *et al.*, 1992). Northern hybridization experiments revealed that the *gl*CK gene is primarily expressed in *G. lamblia* trophozoites and that expression is significantly decreased during encystation (Minotto *et al.*, 1999). The *gl*CK gene is also one of eight genes whose expressions are up-regulated in neomycin-selected *G. lamblia* cell lines (Su *et al.*, 2007), suggesting its importance under stress conditions. The *G. lamblia* arginine deiminase and ornithine transcarbamoylase have recently been purified and functionally characterized in our laboratory (Galkin *et al.*, 2009; Li *et al.*, 2009). Here, we show that *gl*CK is essential for the viability of *G. lamblia* WB trophozoites and

Table 1
Steady-state kinetic parameters.

Substrate	K_m (μM)	k_{cat} (s^{-1})	k_{cat}/K_m ($s^{-1}\,M^{-1}$)
ATP†	35 ± 2	—	—
Carbamate‡	$43 \times 10^3 \pm 11 \times 10^3$	43 ± 7	1.0×10^3
Carbamoyl phosphate§	85 ± 6	319 ± 9	3.8×10^6
ADP¶	70 ± 5	319 ± 9	4.6×10^6

† Reactions contained 30 m*M* ammonium carbamate and 11.5 m*M* $MgCl_2$. Because the carbamate was not saturating (*i.e.* tenfold K_m) in the reaction mixture, the value of the observed k_{cat} of $16.1 \pm 0.3\ s^{-1}$ is less than the actual k_{cat} and is therefore not reported in the table. The use of high concentrations of ammonium carbamate caused inhibition. ‡ Reactions contained 3.5 m*M* ATP, 15 m*M* $MgCl_2$ and a variable amount of NH_4Cl and $KHCO_3$. NH_4Cl and $KHCO_3$ were added as a mixture that had been kept at ambient temperature for 20 min to allow equilibration with carbamate. The carbamate concentration was calculated using the published equilibrium constant (Marshall & Cohen, 1966). § Reactions contained 5 m*M* ADP and a variable amount of carbamoyl phosphate. ¶ Reactions contained 2 m*M* carbamoyl phosphate and a variable amount of ADP.

we also report the purification and structural and functional characterization of the enzyme. The essentiality of *gl*CK together with its absence in humans makes the enzyme an attractive candidate for anti-*Giardia* drug development.

2. Experimental procedures

2.1. Gene cloning, protein expression and purification

Trophozoites of *G. lamblia* isolate WB were grown as described previously (Wieder *et al.*, 1983). The genomic DNA was isolated using the DNA STAT kit (Stratagene). The gene encoding *gl*CK was amplified using *Pfu* Turbo DNA polymerase (Stratagene), genomic DNA and 5′-end and 3′-end primers. The PCR product was inserted into the pDEST-HisMBP expression vector as described previously (Nallamsetty *et al.*, 2005). For protein production, *gl*CK was expressed in *Escherichia coli* strain BL21 (DE3) Star as a maltose-binding protein (MBP) fusion product. Cells were grown in Overnight Express Instant TB autoinduction medium (Novagen) for 20 h at 303 K. The cells were lysed by sonication and the soluble fraction was chromatographed on an Ni–NTA affinity column. After elution and concentration, the *gl*CK MBP-fusion protein was chromatographed on a preparative Sephacryl 100 size-exclusion column. MBP was removed by treatment of the fusion protein with tobacco etch virus (TEV) protease (Nallamsetty *et al.*, 2004) at a molar ratio of 60:1, followed by chromatography on an Ni–NTA affinity column to remove MBP and uncleaved protein. The protein was further purified by ion-exchange chromatography on Source 15Q columns (Amersham Biosciences). Fractions containing protein were collected, dialyzed against 50 m*M* Tris–HCl pH 7.5 and 50 m*M* NaCl and concentrated to 45 mg ml^{-1}. Protein integrity and purity was assessed by polyacrylamide gel electrophoresis in the presence of SDS. The oligomeric state was measured by analytical size-exclusion chromatography on an ÄKTA Purifier 10 using a Superdex-200 HR 10/30 column (Amersham Biosciences).

2.2. Functional knockdown of the CK gene in *G. lamblia*

The *gl*CK gene was inserted into the plasmid between two opposite tetracycline-inducible Ras-related nuclear protein (*ran*) promoters as described previously (Touz *et al.*, 2004). Accordingly, the dsRNA was synthesized from a DNA template upon induction with tetracycline at a final concentration of 10 µg ml^{-1}. Stable transfections of *G. lamblia* trophozoites were produced by electroporation of circular plasmids containing a puromycin-resistance gene. Approximately 10^7 trophozoites were resuspended in 0.3 ml medium, mixed with 10 µg DNA and incubated on ice for 5 min. Cells were electroporated in a 0.4 cm cuvette with an ECM 600 (BTX, San Diego, California, USA) set to 350 V, 1000 µF and 720 Ω and transferred to 15 ml medium in a glass tube after 10 min on ice. After overnight incubation without puromycin, cultures were chilled on ice and additional media and drug were added to a final volume of 20 ml and 100 µ*M* puromycin. Cells were then distributed into a 96-well plate and sealed in an anaerobic environment.

Table 2
X-ray data-collection and refinement statistics.

Values in parentheses are for the highest resolution shell.

Space group	$P2_1$
Crystal solvent content (%)	43
No. of molecules in asymmetric unit	4
Data collection	
Unit-cell parameters (Å, °)	$a = 69.77$, $b = 85.41$, $c = 102.1$, $\beta = 106.8$
Resolution range (Å)	20–3.0 (3.1–3.0)
No. of observations	103189
No. of unique reflections	20419
Completeness (%)	88.4 (87.0)
R_{merge}†	0.095 (0.193)
Refinement statistics	
No. of refined reflections	18918 (1193)
No. of reflections in R_{free} set	998 (70)
Resolution range (Å)	10–3.0 (3.07–3.0)
No. of residues	1161
R_{cryst}‡	0.227 (0.239)
R_{free}§	0.283 (0.381)
R.m.s. deviations	
Bonds (Å)	0.018
Angles (°)	2.1
Backbone dihedral angle distribution (%)	
Allowed	95.3
Generously allowed	4.7
Disallowed	0.0
$\langle B \rangle$ (Å^2)	38.4

† $R_{merge} = \sum_{hkl}\sum_i |I_i(hkl) - \langle I(hkl)\rangle| / \sum_{hkl}\sum_i I_i(hkl)$. ‡ $R_{cryst} = \sum_{hkl} \big||F_{obs}| - |F_{calc}|\big| / \sum_{hkl} |F_{obs}|$, where F_{obs} and F_{calc} are the observed and calculated structure factors, respectively § R_{free} is computed for 5% of reflections that were randomly selected and omitted from the refinement.

2.3. Steady-state kinetics

For the conversion of ATP and ammonium carbamate to ADP and carbamoyl phosphate, reaction solutions (1 ml) initially contained ATP at varied concentration (0.5-fold to fivefold K_m) and 30 m*M* ammonium carbamate (or ammonium carbamate at varied concentrations and 3.5 m*M* ATP), *gl*CK, 3 m*M* PEP, 11.5 m*M* $MgCl_2$, 0.2 m*M* NADH, 10 U lactate dehydrogenase and 10 U pyruvate kinase in 50 m*M* Tris–HCl pH 7.5 at 298 K. The progress of the reaction was monitored at 340 nm ($\Delta\varepsilon = 6.2\ mM^{-1}\ cm^{-1}$). The initial velocities (V_0) measured as a function of the concentration of the varied substrate, [*S*], were fitted with *KinetAsyst* to the equation $V_0 = V_{max}[S]/(K_m + [S])$ to obtain the maximum velocity (V_{max}) and the Michaelis constant (K_m). k_{cat} was calculated from the ratio of the V_{max} and the enzyme concentration.

For the conversion of ADP and carbamoyl phosphate to ATP and ammonium carbamate, reaction solutions (1 ml) initially contained ADP at varied concentrations (0.5-fold to fivefold K_m), 2 m*M* carbamoyl phosphate (or carbamoyl phosphate at varied concentration and 5 m*M* ADP), *gl*CK, 2 m*M* D-glucose, 200 µ*M* NADP, 10 U hexokinase, 5 U glucose-6-phosphate dehydrogenase, 0.002%(*w*/*v*) bovine serum albumin and 30 m*M* $MgCl_2$ in 20 m*M* Tris–HCl pH 8.3 at 310 K. The reaction progress was monitored at 340 nm ($\Delta\varepsilon = 6.2\ mM^{-1}\ cm^{-1}$). The k_{cat} and K_m values were calculated from the initial velocity data as described above and are given in Table 1.

The competitive inhibition constants for adenosine, adenosine 5′-monosulfate and AMPPNP were determined by fitting the initial velocities measured for the ATP-producing reaction in the presence of varied concentrations of the compound examined. The initial velocity data were analyzed using the equation $V_0 = V_{max}[S]/\{K_m(1 + [I]/K_i) + [S]\}$, where K_i is the inhibition constant and $[I]$ is the concentration of the compound.

2.4. Crystallization, data collection and structure determination

The following commercially available crystallization kits were screened: Crystal Screen, Crystal Screen 2, PEG/Ion and PEG/Ion 2 from Hampton Research, Wizard I and Wizard II from Emerald BioSystems and JCSG Core Suite I from Qiagen. The PEG/Ion screen yielded the best crystals. Optimized crystals of *gl*CK were obtained at 293 K by the vapor-diffusion method in hanging drops. The protein solution was mixed with an equal volume of mother liquor containing 20% PEG 3350 and 0.2 *M* ammonium citrate and equilibrated against the mother-liquor reservoir. The crystals were transferred to mother liquor containing 20% glycerol and flash-cooled at 160 K. Diffraction data were acquired using an R-AXIS IV^{++} image-plate detector mounted on a Rigaku rotating-anode MicroMax-007 X-ray generator (Rigaku MSC Inc.). The crystals diffracted X-rays to a resolution of 3.0 Å. Data processing was carried out using *CrystalClear* v.1.3.6 (Rigaku MSC Inc.). The statistics of data collection are provided in Table 2.

The crystal structure of *gl*CK was determined by molecular-replacement techniques using the program *Phaser* (McCoy *et al.*, 2005), with the *Pyrococcus furiosus* CK (*Pf*CK) structure (Ramon-Maiques *et al.*, 2000; PDB code 1e19) as a search model. The difference Fourier maps indicated some alternative polypeptide tracing, which was rebuilt on a graphics workstation using the program *O* (Kleywegt & Jones, 1999). Structure refinement was carried out using *CNS* (Brünger *et al.*, 1998) and *REFMAC* (Murshudov *et al.*, 1997). The resulting models were inspected and modified on a graphics workstation. Given the low resolution of the diffraction, group temperature factors were used (with two groups per amino-acid residue) and no water molecules were included in the model. Refinement statistics are provided in Table 2.

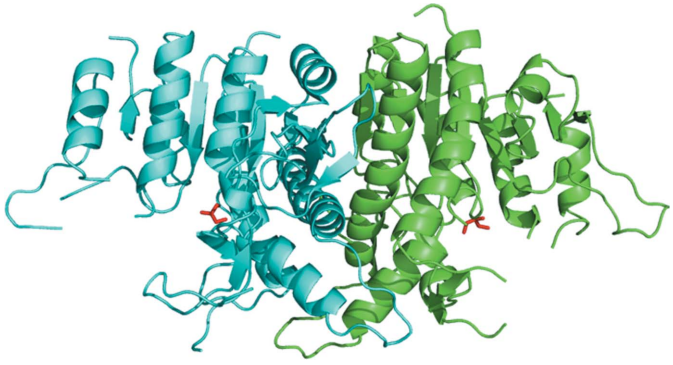

Figure 1
Overall fold of *gl*CK. A ribbon-diagram representation of the protein dimer is shown. Each subunit is represented in a different color. The glycerol molecules in the active sites are shown in red.

3. Results and discussion

3.1. Expression, purification and kinetic properties of *gl*CK

The N-terminally His-tagged MBP-fusion *gl*CK was expressed in soluble form in *E. coli* and remained soluble after digestion with TEV protease and removal of the MBP. Analytical size-exclusion chromatography of purified *gl*CK indicated that the protein primarily exists as a homodimer in solution. ATP/AMP analogs were found to be weak binding inhibitors, with K_i values of 8.5 m*M* for adenosine, 5 m*M* for adenosine 5′-monosulfate and 0.8 m*M* for AMPPNP. Although AMPPNP is a rather weak inhibitor of *gl*CK, it is the best inhibitor reported to date.

3.1.1. *gl*CK essentiality test. Previous experiments have confirmed that the CK gene is functional in *G. lamblia* trophozoites and that *gl*CK is expressed *in vivo* (Minotto *et al.*, 1999; Schofield *et al.*, 1992). To further validate *gl*CK as a potential drug-target candidate, we tested the essentiality of the *gl*CK gene by using the RNAi gene-silencing technique (Bernstein *et al.*, 2001), which has recently been adopted for *G. lamblia* trophozoites (Touz *et al.*, 2004). We have previously used this approach to validate the *G. lamblia* arginine

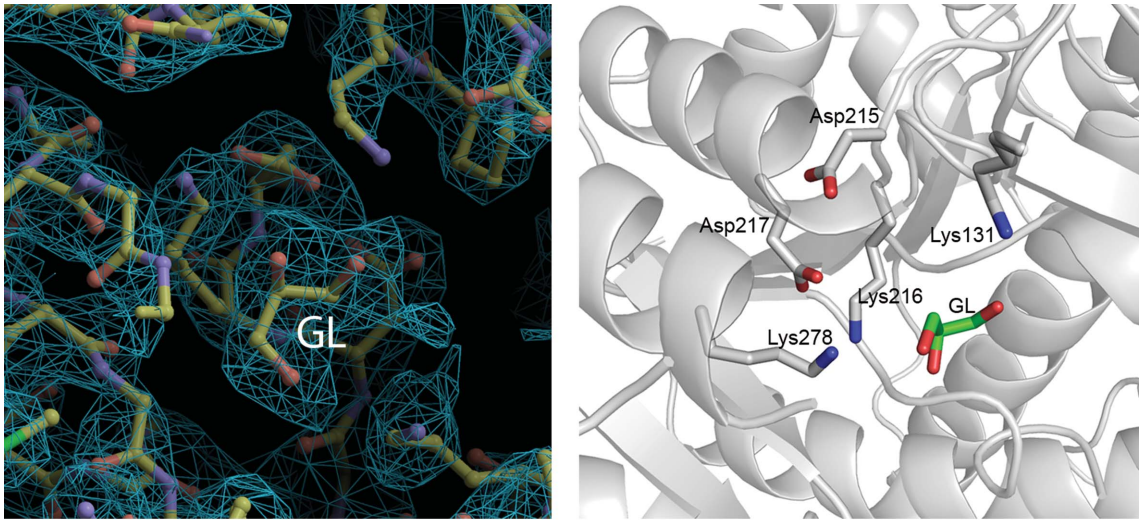

(*a*) (*b*)

Figure 2
View of the *gl*CK active site. (*a*) The σ_A-weighted $2F_o - F_c$ difference Fourier electron-density map in the vicinity of the glycerol molecule (labeled GL) calculated omitting the ligand from the model. Atomic colors are as follows: carbon, yellow; oxygen, red; nitrogen, blue; sulfur, green. (*b*) The lysine and aspartic acid cluster in the vicinity of the glycerol molecule. Atomic colors are as follows: carbon, gray (*gl*CK) and green (glycerol, labeled GL); oxygen, red; nitrogen, blue.

deiminase and fructose-1,6-bisphosphate aldolase as potential drug targets (Li *et al.*, 2009; Galkin *et al.*, 2007). The *G. lamblia* trophozoites were transfected with the *gl*CK gene as described above. No viable trophozoites were observed after 10 d of cultivation. In a control experiment using a nonessential gene encoding the adaptor protein involved in protein trafficking (Touz *et al.*, 2004), viable trophozoites were observed after transfection. The *gl*CK dsRNA triggered transcriptional inhibition and *gl*CK gene silencing, which was lethal for all trophozoites, consistent with the essential role that the enzyme plays in the survival of the parasite.

3.2. Overall structure of glCK

The *gl*CK crystal contains four protein molecules in the asymmetric unit (labeled *A*, *B*, *C* and *D* in the PDB entry) that pack into two homodimers consistent with the oligomeric form in solution. The dimer is depicted in Fig. 1. Two archeal CKs with known structures, *Pf*CK and *Aeropyrum pernix* CK (*ap*CK; K. Shimizu & N. Kunishima, unpublished work; PDB code 2e9y), and a bacterial enzyme from *Enterococcus faecalis* (*Ef*CK) also form dimers (Durbecq *et al.*, 1997; Marina *et al.*, 1999; Ramon-Maiques *et al.*, 2000).

The model of the four *gl*CK molecules in the asymmetric unit includes 1161 of the 1264 amino-acid residues. A glycerol molecule originating from the cryoprotecting solution is located in each active site in a position where the carbamoyl phosphate is expected to bind (Fig. 2*a*). Missing from each of the four molecules are residues that have no associated electron density: the N-terminal residue remaining after TEV protease cleavage (Gly) and the authentic N-terminal Met residue. In addition, no electron density is associated with the following surface residues: 18–19, 135–160 and 272–273 in molecule *A*, 138–152, 244–245 and 271–272 in molecule *B*, 138–161 and 247–250 in molecule *C*, and 140–152, 243–249 and 271–272 in molecule *D*. These residues were omitted from the final model.

The *gl*CK molecule folds into a three-layer $\alpha/\beta/\alpha$ sandwich with parallel open β-sheets surrounded by α-helices, forming a modified 'Rossmann fold' as observed in the structures of the related bacterial CK (Marina *et al.*, 1999). The *gl*CK subunit consists of N-terminal (residues 2–228) and C-terminal (residues 229–316) domains. As in other CKs, the N-terminal domains are positioned in the center of the dimer, thus mediating the intersubunit interface. A *DALI* (Holm & Sander, 1993) search identified three CK structures similar to *gl*CK: *pf*CK (PDB code 1e19; Ramon-Maiques *et al.*, 2000; *Z* score of 39.4; r.m.s.d. of 1.7 Å for 282 aligned C^{α} atoms that share 50% sequence identity), *ef*CK (PDB code 1b7b; Marina *et al.*, 1999; *Z* score of 38.2; r.m.s.d. of 1.5 Å for 278 aligned C^{α} atoms that share 43% sequence identity) and *ap*CK (PDB code 2e9y; K. Shimizu & N. Kunishima, unpublished work; *Z* score of 39.2; r.m.s.d. of 1.7 Å for 282 aligned C^{α} atoms that share 40% sequence identity).

3.3. Active site of *gl*CK

The *gl*CK active site is of special interest for the development of inhibitors which might lead to therapeutic agents. The large crevice between the N- and C-terminal domains of *pf*CK hosts the site for Mg^{2+}-ADP (Ramon-Maiques *et al.*, 2000). A sulfate ion binds at the bottom of the active-site crevice of the *ef*CK structure, occupying a site that is expected to bind the γ-phosphate of ATP or the phosphate group of carbamoyl phosphate (Marina *et al.*, 1999). A strong peak was found in the *gl*CK electron-density map in close proximity to the postulated *ef*CK sulfate ion. Because of the shape of the electron density and the lack of sulfate in the crystallization solution of *gl*CK, the electron density was modeled as a glycerol molecule (Fig. 2). The environment of both the *ef*CK sulfate ion and the *gl*CK glycerol includes the backbone amides of two conserved glycine residues (Gly13 and Gly56 in the *gl*CK sequence) as well as the side chains of five more conserved residues (Lys131, Lys216, Lys278, Asp215 and Asp217; Fig. 2*b*). The bound sulfate in *ef*CK was proposed to occupy the site of the ATP γ-phosphate, the group that is transferred to generate carbamoyl phosphate (Marina *et al.*, 1999). The *gl*CK structure reveals that this site also accommodates a glycerol molecule, a noncharged polar moiety with the potential to donate or accept hydrogen bonds. Superposition of the *gl*CK structure and that of the *pf*CK–Mg^{2+}-ADP complex suggests that if a carbamoyl phosphate binds in the glycerol site its phosphate may be positioned in line to be transferred to the ADP β-phosphate and to generate a pentavalent phosphorus intermediate/transition state (Fig. 3). This transient adduct would have a trigonal bipyramidal geometry with the phosphoryl donor and acceptor groups located at apical positions (Knowles, 1980). The model does not require adjustment of the protein structure and suggests that three invariant lysine residues (Lys131, Lys216 and Lys278) may be involved in substrate binding and phosphoryl transfer (Fig. 3). Lys278 may interact with the ADP β-phosphate to position the substrate for optimal phosphate transfer. Lys216 may interact with the carbamoyl phosphate to counter a negatively charged pentavalent phosphorus intermediate, which has also been suggested for the equivalent *pf*CK Lys215 (Ramon-Maiques *et al.*, 2000). It is noteworthy that the correct positioning of Lys216 for catalysis is ensured by two invariant aspartate residues (Asp215 and Asp217). When the equivalent aspartate residues of *ef*CK (Asp208 and Asp210) were replaced by alanine residues, the

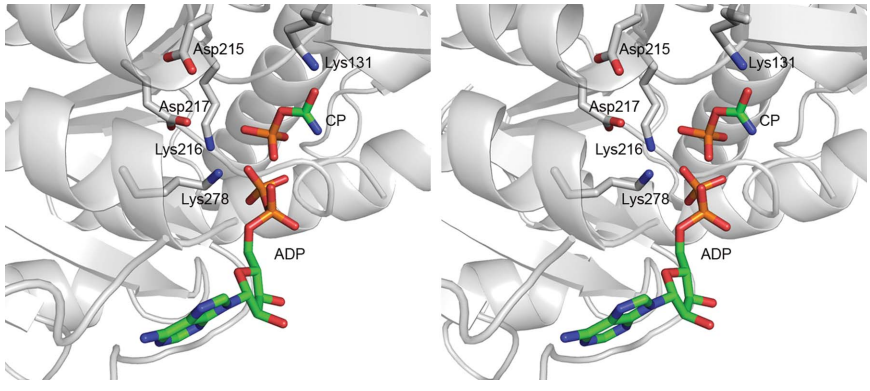

Figure 3
Stereoscopic view of the *gl*CK active site with modeled Mg^{2+}-ADP and carbamoyl phosphate. The Mg^{2+}-ADP was modeled by analogy to that observed in the *pf*CK structure (Ramon-Maiques *et al.*, 2000). The same color scheme is used for carbon, oxygen and nitrogen as in Fig. 2(*b*); P atoms are colored orange.

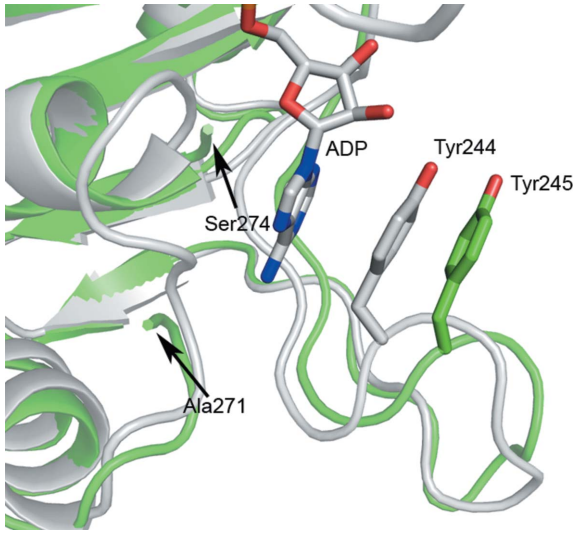

Figure 4
Superposition of *gl*CK (green) and *pf*CK (gray) showing the environment of the adenine group of ADP. A tyrosine-carrying loop adopts a more closed conformation in *pf*CK than in *gl*CK such that the tyrosine residue stacks against the adenine ring. A loop that flanks the other side of the adenine ring is partially disordered in the crystal structure of *gl*CK, which does not contain ADP.

activity of the mutants was reduced by 1000-fold compared with the wild-type enzyme (Marina *et al.*, 1999). The electrostatic network that supports the reaction center is further extended: the carboxyl group of Asp217 interacts with the amino groups of both the conserved Lys278 and Lys216 and the carboxyl group of Asp215 forms hydrogen bonds to the backbone amides of Asp217 and Leu218. The third invariant active-site lysine residue, Lys131, may interact with the carbamoyl O atom of carbamoyl phosphate and fine-tune the orientation of the substrate for efficient phosphate transfer.

Comparison of *gl*CK with *pf*CK revealed intriguing conformational changes associated with the binding of the adenine moiety of ADP (Fig. 4). ADP binding promotes loop closure and a shift in the position of a tyrosine side chain so that the aromatic ring stacks against the adenine ring. The second difference is the disorder of the loop residues 272–273 in the absence of ADP.

Site-directed mutagenesis experiments together with structures of liganded *gl*CK will provide better insight into the CK reaction mechanism and strategies for inhibitor development.

This work was supported by a grant from the National Institutes of Health (R01 AI059733).

References

Adam, R. D. (2001). *Clin. Microbiol. Rev.* **14**, 447–475.
Bernstein, E., Denli, A. M. & Hannon, G. J. (2001). *RNA*, **7**, 1509–1521.
Biagini, G. A., Yarlett, N., Ball, G. E., Billetz, A. C., Lindmark, D. G., Martinez, M. P., Lloyd, D. & Edwards, M. R. (2003). *Mol. Biochem. Parasitol.* **128**, 11–19.
Brünger, A. T., Adams, P. D., Clore, G. M., DeLano, W. L., Gros, P., Grosse-Kunstleve, R. W., Jiang, J.-S., Kuszewski, J., Nilges, M., Pannu, N. S., Read, R. J., Rice, L. M., Simonson, T. & Warren, G. L. (1998). *Acta Cryst.* D**54**, 905–921.
Durbecq, V., Legrain, C., Roovers, M., Pierard, A. & Glansdorff, N. (1997). *Proc. Natl Acad. Sci. USA*, **94**, 12803–12808.
Galkin, A., Kulakova, L., Melamud, E., Li, L., Wu, C., Mariano, P., Dunaway-Mariano, D., Nash, T. E. & Herzberg, O. (2007). *J. Biol. Chem.* **282**, 4859–4867.
Galkin, A., Kulakova, L., Wu, R., Gong, M., Dunaway-Mariano, D. & Herzberg, O. (2009). *Proteins*, **76**, 1049–1053.
Holm, L. & Sander, C. (1993). *J. Mol. Biol.* **233**, 123–138.
Kleywegt, G. J. & Jones, T. A. (1999). *Acta Cryst.* D**55**, 941–944.
Knodler, L. A., Sekyere, E. O., Stewart, T. S., Schofield, P. J. & Edwards, M. R. (1998). *J. Biol. Chem.* **273**, 4470–4477.
Knowles, J. R. (1980). *Annu. Rev. Biochem.* **49**, 877–919.
Li, Z., Kulakova, L., Li, L., Galkin, A., Zhao, Z., Nash, T. E., Mariano, P. S., Herzberg, O. & Dunaway-Mariano, D. (2009). *Bioorg. Chem.* **37**, 149–161.
Marina, A., Alzari, P. M., Bravo, J., Uriarte, M., Barcelona, B., Fita, I. & Rubio, V. (1999). *Protein Sci.* **8**, 934–940.
Marshall, M. & Cohen, P. P. (1966). *J. Biol. Chem.* **241**, 4233–4242.
McCoy, A. J., Grosse-Kunstleve, R. W., Storoni, L. C. & Read, R. J. (2005). *Acta Cryst.* D**61**, 458–464.
Minotto, L., Tutticci, E. A., Bagnara, A. S., Schofield, P. J. & Edwards, M. R. (1999). *Mol. Biochem. Parasitol.* **98**, 43–51.
Murshudov, G. N., Vagin, A. A. & Dodson, E. J. (1997). *Acta Cryst.* D**53**, 240–255.
Nallamsetty, S., Austin, B. P., Penrose, K. J. & Waugh, D. S. (2005). *Protein Sci.* **14**, 2964–2971.
Nallamsetty, S., Kapust, R. B., Tozser, J., Cherry, S., Tropea, J. E., Copeland, T. D. & Waugh, D. S. (2004). *Protein Expr. Purif.* **38**, 108–115.
Palm, J. E., Weiland, M. E., Griffiths, W. J., Ljungstrom, I. & Svärd, S. G. (2003). *J. Infect. Dis.* **187**, 1849–1859.
Ramon-Maiques, S., Marina, A., Uriarte, M., Fita, I. & Rubio, V. (2000). *J. Mol. Biol.* **299**, 463–476.
Schofield, P. J., Edwards, M. R., Matthews, J. & Wilson, J. R. (1992). *Mol. Biochem. Parasitol.* **51**, 29–36.
Su, L.-H., Lee, G. A., Huang, Y.-C., Chen, Y.-H. & Sun, C.-H. (2007). *Mol. Biochem. Parasitol.* **156**, 124–135.
Touz, M. C., Kulakova, L. & Nash, T. E. (2004). *Mol. Biol. Cell*, **15**, 3053–3060.
Wieder, S. C., Keister, D. B. & Reiner, D. S. (1983). *J. Parasitol.* **69**, 1181–1182.